Double Ionization of Helium in Extreme Ultraviolet Pulse in Presence of Extremely Short Mid-Infrared Pulse

Xu Liang[1], Wu Wanyang[1], He Feng[1,2*]

[1] *Key Laboratory for Laser Plasmas (Ministry of Education) and School of Physics and Astronomy, Shanghai Jiao Tong University, Shanghai* 200240, *China*

[2] *Collaborative Innovation Center of IFSA (CICIFSA), Shanghai Jiao Tong University, Shanghai* 200240, *China*

Abstract The double ionization of helium in the combined extreme ultraviolet (EUV) pulse and extremely short mid-infrared (MIR) laser pulse is studied by numerically simulating the time-dependent Schrödinger equation. In this process, the EUV pulse kicks off one electron, and then the produced He^+ is either sequentially tunneling ionized by the remaining MIR pulse, or nonsequentially impact ionized by the rescattering electron driven by the MIR laser pulse. The interference of the coexisted sequential and nonsequential double ionization events produces an unexplored electron-electron joint momentum distribution. The two electrons released via rescattering may propagate along the same direction and also propagate along the opposite directions when such an extremely short laser pulse is implemented.

Key words ultrafast optics; double ionization; momentum spectrum; helium

OCIS codes 320.7120; 320.7150; 020.2649; 020.4180

氦原子在超短中红外脉冲和极紫外光场作用下的双电离

许亮[1], 吴婉阳[1], 何峰[1,2*]

[1] 上海交通大学物理与天文学院激光等离子体教育部重点实验室, 上海 200240

[2] 上海交通大学 IFSA 协同创新中心, 上海 200240

摘要 利用数值求解含时薛定谔方程的方法研究了氦原子在超短红外激光脉冲和极紫外激光场作用下的双电离过程。在此过程中,一个电子首先被极紫外激光场电离,然后氦离子既可以被接下来的红光激光场直接隧穿电离,也可以被红外激光场驱动下的电子再散射而发生非次序双电离。这两种双电离通道的干涉可以产生新颖的电子关联动量谱分布。当驱动红外激光脉冲为周期量级时,再散射导致的双电离的两个电子的运动方向可以相同,也可以相反。

关键词 超快光学; 双电离; 动量谱; 氦原子

中图分类号 O562.4; O562.5 **文献标识码** A **doi**: 10.3788/CJL201946.0508022

1 Introduction

Thanks to the great advances of ultrashort laser technologies, ionization of atoms and molecules in strong laser fields has been extensively studied in past decades. On the basis of the understanding of single ionization, which can be grouped into multiphoton ionization[1-2] or tunneling ionization[3-5] according to the Keldysh parameter[6], double ionization has also attracted attention during the past years. As the simplest two-electron system, the helium atom has worked as a prototypical system for understanding double ionization, as well as the multi-electron atom Mg[7-8]. When a helium atom is exposed to extreme ultraviolet (EUV) pulses, one electron may absorb high energetic photons and escape from the parent ion,

收稿日期: 2019-01-15; **修回日期**: 2019-03-03; **录用日期**: 2019-03-11

基金项目: 国家重点研发计划(2018YFA0404802)、国家自然科学基金(11574205, 11721091, 91850203)、上海市教育委员会科研创新计划(2017-01-07-00-02-E00034)、上海市曙光项目(17SG10)

* **E-mail**: fhe@sjtu.edu.cn

meanwhile the bound electron is shook off[9]. The atom may simultaneously absorb two photons if one is not enough, and the photon energies are shared by the two freed electrons[10]. For a helium atom in intense long-wavelength laser fields, the concept of field ionization is more vivid. In this case, the two electrons may eject in two independent single ionization processes[11], which is termed as "sequential double ionization" (SDI). Alternatively, the two electrons may be also stripped off via nonsequential double ionization (NSDI), i.e., one electron tunnels out of the laser-distorted Coulomb potential, and later rescatters with its parent ion, ultimately resulting in double ionization. Depending on the rescattering energy, the second electron may be kicked off directly, identified as recollision-impact ionization (RII), or be pumped to some excited states, which will be tunneling ionized in the remaining laser field, as termed as recollision excitation with subsequent ionization (RESI)[12-13]. NSDI can be described reasonably well by the recollision model[14]. The SDI and NSDI dominate in different laser intensity ranges. Sometimes, the ionized electron that does not gain sufficient drift momentum in this process would be recaptured by the Coulomb attracting potential and eventually be trapped into the high-lying Rydberg states, which we called as "frustrated tunneling ionization (FTI)"[15-16].

In the two-electron joint momentum distribution, RII contributes to the momentum distribution in the first and third quadrants[17-19]. As intensities are below or close to the recollision threshold, anticorrelation between the electrons has been observed[20-22]. Electron anticorrelation was basically explained within the mechanisms of recollision-induced-excitation tunneling and multiple-recollision[23-25]. The recollision-induced-excitation tunneling mechanism always prefers to cause back-to-back emission[24]. In the multiple-recollision case, the ionization events uniformly distribute in the four quadrants of the electron-electron momentum distribution diagram[26], and the sum-energy spectrum of two electrons can be fitted with the Maxwellian distribution[27]. If several excited states are mediated in the double ionization process, the interference from different excitation channels will break the fourfold symmetry of the RESI distributions[28].

In spite of many intriguing phenomena discovered in the double ionization, some questions still remain open. For example, may NSDI and SDI coexist and interfere with each other in some laser conditions? Are there some new phenomena for the double ionization if the driving laser pulse is extremely short?

The theoretical study of double ionization of helium or other more complex systems relies on the numerical simulation of the time-dependent Schrödinger equation, or the strong field approximation, or even time-dependent perturbation theory if only few photons are involved. The fully dimensional time-dependent Schrödinger equation (TDSE) simulation for helium in infrared or MIR laser fields is still overloaded for supercomputers. However, the reduced dimensional TDSE can capture the main dynamics and thus is still used in many research[29-33]. In this paper, we numerically simulate the TDSE by confining both electrons moving along the laser polarization axis and study the correlated and anticorrelated electron joint momentum distributions. Physically, one electron absorbs a high-energetic EUV photon and gets released, and the MIR field may drive it back to He^+, resulting in the NSDI. Alternatively, after the single ionization of He, the new produced He^+ may be further tunneling ionized directly by the MIR field, resulting in the SDI. The interference of NSDI and SDI is expected and demonstrated in the correlated joint electron momentum distribution. Surprisingly, the two electrons freed via rescattering may also propagate oppositely.

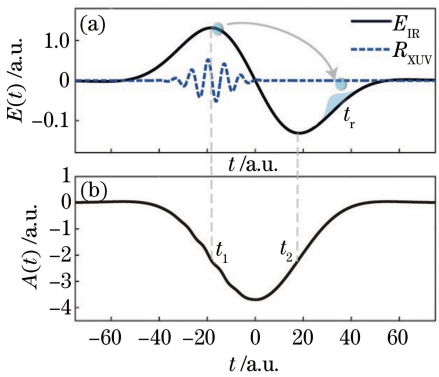

Fig. 1　Combined laser fields as a function of time. (a) IR and EUV laser electric fields; (b) vector potential of the combined laser fields. The IR pulse has the wavelength 800 nm and the intensity $I_1 = 1.5 \times 10^{15}$ W/cm^2. Time delay is $t_d = -17$ a.u.

2　Numerical models

We have performed *ab initio* numerical simulations using a two-dimensional model, where the motion of both electrons is restricted to the laser polarization direction. This model has been used to reproduce many NSDI features[18,34-35]. The Hamiltonian is given by (atomic units are used throughout unless stated otherwise)

$$H(t) = H_0 + H_{int}(t), \tag{1}$$

as a sum of the field-free Hamiltonian H_0 and the laser-electron interaction H_{int}. The time evolution of the wave packet was calculated according to the following integral equation[36-38]:

$$\Psi(t)=-\mathrm{i}\int_{-\infty}^{t}\exp\left[-\mathrm{i}\int_{\tau}^{t}H(t')\mathrm{d}t'\right]H_{\mathrm{int}}(\tau)\times\exp(-\mathrm{i}H_0\tau)\Phi_0\mathrm{d}\tau+\exp(-\mathrm{i}H_0t)\Phi_0,\quad(2)$$

with Φ_0 being the initial wave function. The field-free Hamiltonian is

$$H_0=p_1^2/2+p_2^2/2+V(x_1,x_2),\quad(3)$$

where p_1 and p_2 are the momentum operators for two electrons, respectively, and $V(x_1, x_2)$ is the Coulomb potential describing the electron-electron repulsion and electron-nucleus attraction. The modeled Coulomb potential is written as

$$V(x_1,x_2)=-\sum_{i=1,2}\frac{2}{\sqrt{x_i^2+s_1}}\exp(-x_i^2/m_{\mathrm{en}})+\frac{1}{\sqrt{(x_1-x_2)^2+s_2}}\exp[-(x_1-x_2)^2/m_{\mathrm{ee}}],\quad(4)$$

where m_{en} and m_{ee} are used for screening the electron-nucleus attraction and electron-electron repulsion, respectively. The two soft-core parameters are $s_1=0.5$ and $s_2=0.339$, which guarantee the ground state energies of He and He^+[29] to be -2.9 a.u. and -2.0 a.u. when m_{ee} and m_{en} are both infinitely large.

The laser-electron interaction is expressed in length gauge:

$$H_{\mathrm{int}}(t)=(x_1+x_2)E(t),\quad(5)$$

where $E(t)$ is the combined laser field of E_{EUV} and E_{MIR} which have the forms

$$E_{\mathrm{EUV}}(t)=E_1f_1(t-t_{\mathrm{d}})\cos[\omega_1(t-t_{\mathrm{d}})+\varphi_1],\quad(6)$$

$$E_{\mathrm{MIR}}(t)=E_2f_2(t)\cos(\omega_2t+\pi/2),\quad(7)$$

with a Gaussian envelope $f_j(t)=\exp[-4\ln 2(t/\tau_j)^2]$, where $\tau_1=2.5T_1$ and $\tau_2=0.5T_2$ with T_1 and T_2 being the EUV and MIR periods. t_{d} is the time delay between the two pulses. For a negative delay, the EUV pulse precedes the MIR pulse. The amplitudes are $E_i=\sqrt{I_i/3.51\times10^{16}}$. The EUV intensity is $I_1=10^{14}$ W/cm^2, and the EUV central photon energy is fixed at $\omega_1=0.9$ a.u.. Note that the integration of $E_{\mathrm{MIR}}(t)$ over time yields zero though τ_2 is extremely short.

In simulations, we set the spatial grids $\Delta x_1=\Delta x_2=0.2$ a.u. and the time step $\Delta t=0.05$ a.u.. The simulation box covers the areas $[-1000, 1000]$ a.u. in both directions. We applied a function of $\cos^{1/6}$ form for absorber, and accumulated the ionization probabilities absorbed by the boundaries. The wave function $\Psi(x_1, x_2)$ is symmetric with respect to the exchange of the two electrons because the two electrons are indistinguishable fermions. The double ionization when two electrons propagate in the same or opposite directions is named as correlated or anticorrelated ionization, respectively. In order to analyze the correlated and anticorrelated ionization processes, we partitioned the plane (x_1, x_2) as follows:

correlated: $|x_1|>50$ and $|x_2|>50$ and $x_1x_2>0$,

anticorrelated: $|x_1|>50$ and $|x_2|>50$ and $x_1x_2<0$.

In simulations, we propagated the wave function for an extra 200 a.u. after the laser field vanished in order to wait for all double ionized components to enter the partitioned areas. At the end of propagation, electron-electron momenta and energy spectra of double ionization were obtained by Fourier transforming the wave function distributed in partitioned areas. The initial state Φ_0 in Eq. (2) was obtained by imaginary time propagation[39] in an unscreened Coulomb potential, and the Crank-Nicholson method[40] was used for the wave function propagation.

3 Simulation results

3.1 Correlated double ionization

Figure 1(a) plots the EUV field (dashed curve) and the MIR field (solid curve), and the combined laser vector potential $A(t)=-\int_{-\infty}^{t}E(t')\mathrm{d}t'$ is shown in Fig. 1(b). The time delay t_{d} is -17 a.u.. According to the classical evaluation, the freed electron triggered by the EUV pulse will be driven back to the parent ion at $t_{\mathrm{r}}=39$ a.u. with the rescattering energy of 2.34 a.u..

In the combined EUV and IR field, the double ionization undergoes the following several pathways. Firstly, the electron produced by the EUV field is driven back by the MIR field and rescatters with the He^+ at t_{r} marked in Fig. 1 (a), resulting in the RII. Secondly, one electron is tunneling ionized by the IR field at t_1 when the electric field reaches its first maximum, and the produced He^+ is later tunneling ionized again at t_2 when the second maximum of the IR electric field comes. Thirdly, one electron is released by absorbing the high energetic EUV photon, and the produced He^+ is tunneling ionized by the IR field at t_2, which is abbreviated as EUV-assisted SDI. In simulations, we evaluated double ionization probabilities of the second and third pathways by excluding or including the EUV pulse, and we found that the second pathway contributes significantly smaller ionization probabilities. Actually, the role of the EUV pulse is simply for enhancing the single ionization probability. Thus, we will not discuss the ionization events produced in the second pathway. For the third pathway, two electrons are subsequently released at t_1 and t_2, and finally acquire similar momenta. For extremely short laser pulses, the first and third pathways may contribute the same final photoelectron momenta, and thus these two pathways will interfere with each other.

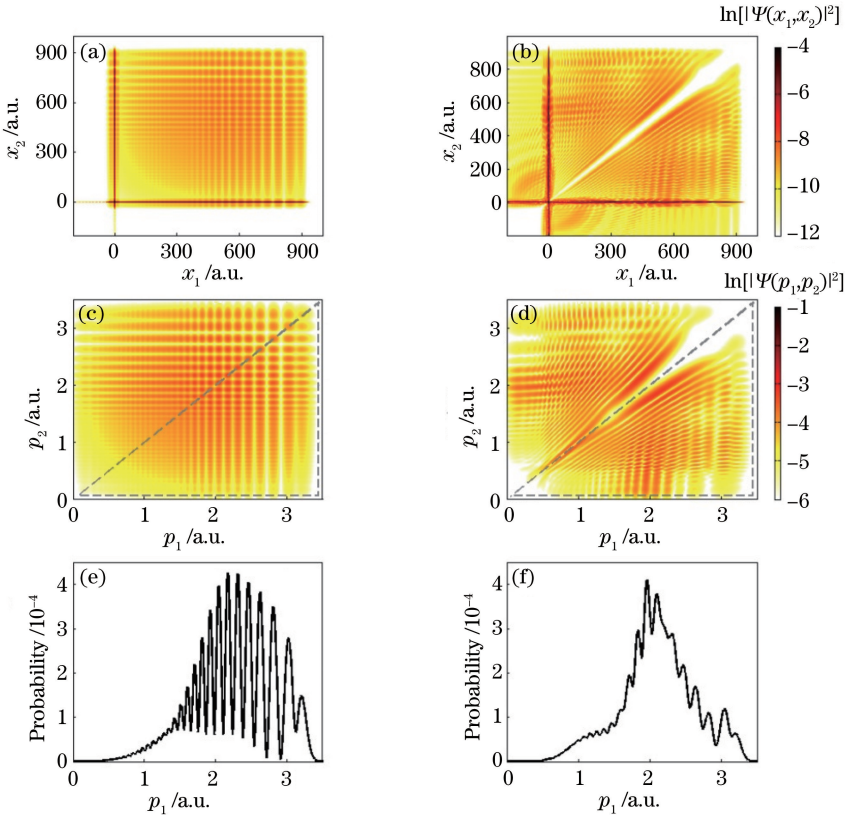

Fig. 2　Correlated information of the electrons. (a) and (b) denote wave functions at time $t=323$ a.u. when the electron-electron repulsion is excluded or included, respectively; (c) momentum distribution of correlated double ionization in (a); (d) momentum distribution of correlated double ionization in (b); (e) and (f) denote the single electron momentum distribution after integrating the signals marked by the triangles in (c) and (d) along the vertical axis, respectively

To disentangle the contributions from the first and third pathways, in which electron-electron correlations are distinct, we tailored $H(t)$ in Eq. (2) by omitting the electron-electron repulsion. By doing this, the rescattering-induced NSDI is excluded. Figure 2(a) shows the two-electron wave function as the electron-electron interaction is omitted, and the corresponding correlated two-electron momentum distribution is shown in Fig. 2(c). The two dimensional lattices in Figs. 2(a) and 2(c) show the characterization of sequential double ionization. By integrating one electron information, one may get a series of peaks in another electron′s momentum spectrum. These peaks are induced by the intracycle interference, i.e., the interference of the single ionization events is ejected at t_1 and t_2 while the laser vector potentials are the same. By keeping the electron-electron repulsion in $H(t)$ in Eq. (2), the NSDI will be very distinct. Figures 2(b) and 2(d) show the two electron distributions in the coordinate and momentum representations, respectively. Compared to the left panels in Fig. 2, the electron-electron repulsion squeezes the distribution off the diagonal line in the first quadrant by forming the distribution with the shape of straight lines. By integrating the momentum in the lower triangles of Figs. 2(c) and 2(d) along the vertical axis, one obtains similar peaks, shown in Figs. 2(e) and 2(f). The similarity of Figs. 2(e) and 2(f) confirms that the EUV-assisted SDI still occurs. The interference of these two pathways results in the joint momentum distribution shown in Fig. 2(d).

3.2　Anticorrelated double ionization

Besides the distinct wave function distribution in the first quadrant in Fig. 2(b), a closer look of Fig. 2(b) gives wave function distributions in the second and fourth quadrants, which is absent in Fig. 2(a). Since the only difference between Figs. 2(a) and 2(b) is the electron-electron correlation, we confirmed the anticorrelated wave function distribution in Fig. 2(b) is contributed by the electron-electron repulsion. This signal is more notable if MIR pulses with longer wavelengths are used. We show the wave function distribution in Fig. 3(a), and the corresponding momentum distribution is shown in Fig. 3(b). The anticorrelated momentum distributions in the second and fourth quadrants yield the two-electron joint energy distribution in Fig. 3(c). The concentric arcs in Figs.

3(a) and 3(b), as well as the straight strips with the slope $k=-1$ in Fig. 3(c), indicate the strong correlation between the two electrons. We should note that the strong correlation in Fig. 3 is different from similar structures in Refs. [34, 41-44]. In those previous works, all of the discrete peaks in sum energies induced by the many-cycle laser field are spaced by integer units of a photon energy. However, in our study at most one rescattering event occurs because the driving laser pulse is ultrashort. After integrating the events that the sum energies for two electrons are constants, we obtained the sum energies spectrum shown in Fig. 3(d). The energy separation between neighboring energy peaks is not constant but depends on the wavelength and intensity of the MIR pulse. With the decreasing of MIR intensities, these concentric rings or straight strips in anticorrelated double ionization would be smoothed or disappear.

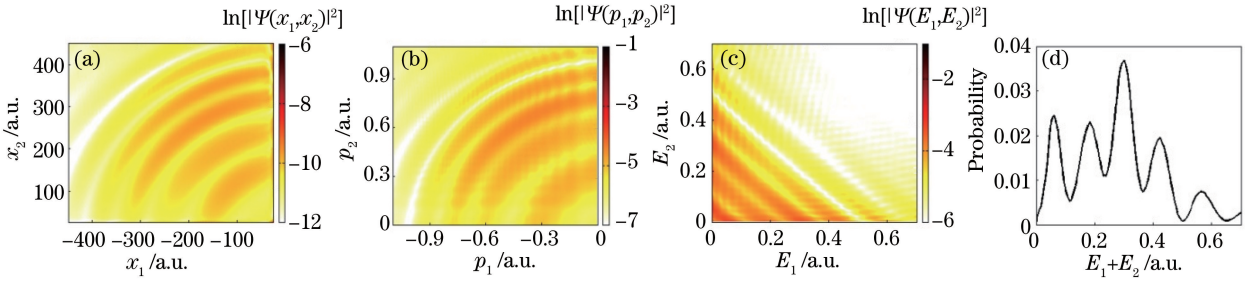

Fig. 3　Correlated information of the electrons. Photoelectron wave function in (a) space and (b) momentum representations at time $t=344$ a.u.; (c) electron-electron joint energy spectrum; (d) sum energy of two electrons obtained by integrating the signals in (c) along the lines $E_1+E_2=$const. The IR wavelength is 1200 nm, and the intensity $I_1=8.3\times10^{14}$ W/cm^2. The time delay is $t_d=-25.5$ a.u.

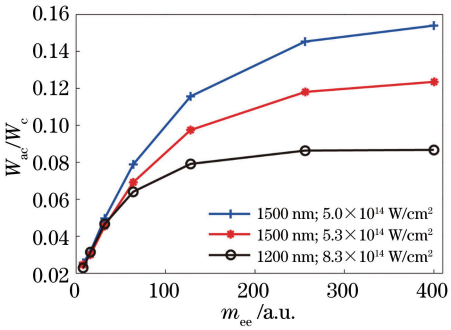

Fig. 4　Ratio (anticorrelated double ionization probability to correlated double ionization probability) as a function of the screening parameter m_{ee}. Other parameters for the line with open circles are the same as those used in Fig. 3. For the line with crosses and line with stars, MIR intensities are $I_1=5\times10^{14}$ W/cm^2 and 5.3×10^{14} W/cm^2. MIR wavelengths are both 1500 nm, and the delay $t_d=-32$ a.u.

We are still not sure how this energy sharing between the oppositely propagating electron pair works. One possible mechanism could be that the rescattering happens when both the electric field and vector potential are close to zero. During the rescattering, the kinetic energy of the freed electron is reallocated between two electrons. However, for a multicycle laser pulse, rescattering occurs when the temporary vector potential is maximum and the subsequent laser field will streak the two freed electrons and thus destroy the concentric arcs.

It is expected that Coulomb interaction between two electrons is important for the anticorrelated momentum distribution. To see how the electron-electron repulsion modifies the electron-electron joint momentum distribution, we screened the electron-electron repulsion by setting a screening factor m_{ee} in Eq. (4). Figure 4 shows the ratio of anticorrelated and correlated double ionization probabilities W_{ac}/W_c. For a very small m_{ee}, the repulsion between two electrons is weak, and thus the two electrons are prone to propagate along the direction in which the rescattering electron holds, i.e., staying in the first quadrant. With the increasing of m_{ee}, the Coulomb repulsion is stronger and stronger, and the ratio increases. It is the Coulomb repulsion that forces one electron to propagate oppositely with the rescattering electron, i.e., going to the second or fourth quadrant.

The ratio presented in Fig. 4 depends on the MIR intensity and wavelength. Comparing the line with crosses and line with stars, we observed that the ratio W_{ac}/W_c is smaller for laser pulses with higher intensities if other parameters are the same. For a stronger laser pulse, the rescattering energy is larger, and thus the two electrons are more prone to propagate along the same direction, leading to a smaller ratio. Comparing the line with stars and the line with open circles, the ratio is smaller for a shorter wavelength even though the rescattering energies are the same for two laser conditions.

In addition to modifying the effective electron-

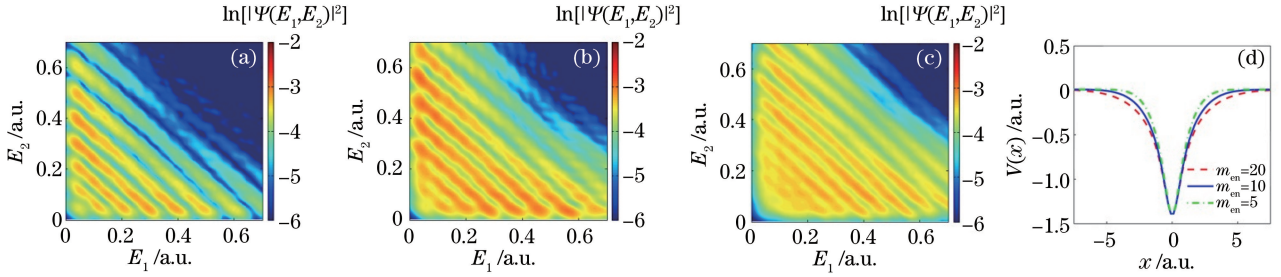

Fig. 5　Anticorrelated joint electron-electron energy spectra. (a), (b) and (c) are joint electron-electron energy spectra for anticorrelated double ionization in the second and fourth quadrants at $m_{en}=20$, 10, 5, respectively; (d) potentials at different screening parameters ($m_{en}=20$, 10, 5). The MIR laser parameters are $\lambda_1=2000$ nm, $I_1=3\times10^{14}$ W/cm^2. Time delay t_d between the two laser pulses is $t_d=-56$ a.u.

electron repulsion, we also studied the influence of the Coulomb attraction between the electron and nucleus. In the potential described in Eq. (4), we screened the Coulomb attraction by modifying m_{en}. Figures 5(a), 5(b) and 5(c) show the joint electron energy spectra of anticorrelated double ionization when $m_{en}=20$, 10 and 5, respectively. Figure 5(d) shows the screened electron-nucleus Coulomb potentials. The overall structures in Figs. 5(a), 5(b) and 5(c) are similar, however, the stripes are denser for smaller m_{en}. In our test calculations, we also looked into the dependence of the joint energy distribution on the rescattering energy by using different MIR intensities and wavelengths. Generally, for larger rescattering energies, the two anticorrelated electrons may ultimately escape. We thus concluded that the anticorrelated momentum distribution depends on Coulomb interactions and rescattering energies.

4　Conclusion

In conclusion, the double ionization triggered by an EUV pulse and an extremely short MIR pulse is studied. For such an extremely short MIR pulse, the rescattering occurs at the tail of the laser pulse, and both freed electrons are not streaked after double ionization. Hence, the nonsequential and sequential double ionization wave packets may interfere with each other. Some slow electrons triggered by rescattering may propagate oppositely though they are strongly correlated. This study shows that the joint electron-electron momentum distribution depends on the Coulomb potentials and rescattering energies.

References

[1] Hurst G S, Payne M G, Kramer S D, *et al*. Resonance ionization spectroscopy and one-atom detection[J]. Reviews of Modern Physics, 1979, 51(4): 767-819.

[2] Javanainen J, Eberly J H, Su Q C. Numerical simulations of multiphoton ionization and above-threshold electron spectra[J]. Physical Review A, 1988, 38(7): 3430-3446.

[3] Tong X M, Zhao Z X, Lin C D. Theory of molecular tunneling ionization[J]. Physical Review A, 2002, 66(3): 033402.

[4] Huang K Y, Xia Q Z, Fu L B. Survival window for atomic tunneling ionization with elliptically polarized laser fields[J]. Physical Review A, 2013, 87(3): 033415.

[5] Pedatzur O, Orenstein G, Serbinenko V, *et al*. Attosecond tunnelling interferometry [J]. Nature Physics, 2015, 11(10): 815-820.

[6] Keldysh L V. Ionization in the field of a strong electromagnetic wave [J]. Soviet Physics JETP, 1965, 20(5): 1307-1314.

[7] Zheng X X, Bai L H, Feng F Z. Non-sequential double ionization of magnesium atom in elliptically polarized strong laser field [J]. Laser & Optoelectronics Progress, 2017, 54(8): 080201.

[8] Feng F Z, Bai L H, Zheng X X. Non-sequential double ionization of Mg atoms below threshold laser power density[J]. Acta Optica Sinica, 2018, 38(7): 0702003.

[9] Carlson T A, Nestor C W Jr. Calculation of electron shake-off probabilities as the result of X-ray photoionization of the rare gases[J]. Physical Review A, 1973, 8(6): 2887-2894.

[10] Jiang W C, Shan J Y, Gong Q H, *et al*. Virtual sequential picture for nonsequential two-photon double ionization of helium [J]. Physical Review Letters, 2015, 115(15): 153002.

[11] Lambropoulos P. Mechanisms for multiple ionization of atoms by strong pulsed lasers[J]. Physical Review Letters, 1985, 55(20): 2141-2144.

[12] Becker W, Liu X J, Ho P J, *et al*. Theories of photoelectron correlation in laser-driven multiple atomic ionization[J]. Reviews of Modern Physics, 2012, 84(3): 1011-1043.

[13] Corkum P B. Recollision physics[J]. Physics Today, 2011, 64(3): 36-41.

[14] Corkum P B. Plasma perspective on strong field multiphoton ionization[J]. Physical Review Letters,

1993, 71(13): 1994-1997.

[15] Zhang W B, Li H, Gong X C, *et al*. Tracking the electron recapture in dissociative frustrated double ionization of D2[J]. Physical Review A, 2018, 98(1): 013419.

[16] Zhang W B, Gong X C, Li H, *et al*. Electron-nuclear correlated multiphoton-route to Rydberg fragments of molecules[J]. Nature Communications, 2019, 10: 757.

[17] Kopold R, Becker W, Rottke H, *et al*. Routes to nonsequential double ionization[J]. Physical Review Letters, 2000, 85(18): 3781-3784.

[18] Lein M, Gross E K U, Engel V. Intense-field double ionization of helium: identifying the mechanism[J]. Physical Review Letters, 2000, 85(22): 4707-4710.

[19] Weber T, Giessen H, Weckenbrock M, *et al*. Correlated electron emission in multiphoton double ionization[J]. Nature, 2000, 405(6787): 658-661.

[20] Liu Y Q, Tschuch S, Rudenko A, *et al*. Strong-field double ionization of Ar below the recollision threshold [J]. Physical Review Letters, 2008, 101(5): 053001.

[21] Liu Y Q, Ye D F, Liu J, *et al*. Multiphoton double ionization of Ar and Ne close to threshold [J]. Physical Review Letters, 2010, 104(17): 173002.

[22] Liu Y Q, Fu L B, Ye D F, *et al*. Strong-field double ionization through sequential release from double excitation with subsequent Coulomb scattering [J]. Physical Review Letters, 2014, 112(1): 013003.

[23] Haan L, Smith S, Shomsky N, *et al*. Anticorrelated electrons from weak recollisions in nonsequential double ionization[J]. Journal of Physics B: Atomic, Molecular and Optical Physics, 2008, 41(21): 211002.

[24] Ye D F, Liu J. Strong-field double ionization at the transition to below the recollision threshold [J]. Physical Review A, 2010, 81(4): 043402.

[25] Shaaran T, Nygren M T, Figueira de Morisson Faria C. Laser-induced nonsequential double ionization at and above the recollision-excitation-tunneling threshold[J]. Physical Review A, 2010, 81(6): 063413.

[26] Zhang Z L, Bai L H, Zhang J T. Double ionization of Ar below the recollision threshold intensity [J]. Physical Review A, 2014, 90(2): 023410.

[27] Ye D F, Li M, Fu L B, *et al*. Scaling laws of the two-electron sum-energy spectrum in strong-field double ionization[J]. Physical Review Letters, 2015, 115(12): 123001.

[28] Maxwell A, de Morisson Faria C F. Controlling below-threshold nonsequential double ionization via quantum interference[J]. Physical Review Letters, 2016, 116(14): 143001.

[29] Zhao J, Lein M. Probing Fano resonances with ultrashort pulses[J]. New Journal of Physics, 2012, 14(6): 065003.

[30] Li Z C, He F. *Ab initio* non-Born-Oppenheimer simulations of rescattering dissociation of H_2 in strong infrared laser fields[J]. Physical Review A, 2014, 90(5): 053423.

[31] Xie X H. Two-dimensional attosecond electron wave-packet interferometry[J]. Physical Review Letters, 2015, 114(17): 173003.

[32] Wu W Y, He F. Asymmetric photoelectron momentum distribution driven by two-color XUV fields[J]. Physical Review A, 2016, 93(2): 023415.

[33] Li Z C, Jaron-Becker A, He F. Superelastic rescattering in single ionization of helium in strong laser fields[J]. Physical Review A, 2016, 94(4): 043406.

[34] Lein M, Gross E K U, Engel V. Discrete peaks in above-threshold double-ionization spectra[J]. Physical Review A, 2001, 64(2): 023406.

[35] Lappas D G, van Leeuwen R. Electron correlation effects in the double ionization of He[J]. Journal of Physics B: Atomic, Molecular and Optical Physics, 1998, 31(6): L249-L256.

[36] Tong X M, Hino K, Toshima N. Phase-dependent atomic ionization in few-cycle intense laser fields[J]. Physical Review A, 2006, 74(3): 031405.

[37] Tong X M, Watahiki S, Hino K, *et al*. Numerical observation of the rescattering wave packet in laser-atom interactions[J]. Physical Review Letters, 2007, 99(9): 093001.

[38] He P L, Takemoto N, He F. Photoelectron momentum distributions of atomic and molecular systems in strong circularly or elliptically polarized laser fields[J]. Physical Review A, 2015, 91(6): 063413.

[39] Kosloff R, Kosloff D. Absorbing boundaries for wave propagation problems[J]. Journal of Computational Physics, 1986, 63(2): 363-376.

[40] Press W H, Teukolsky S A, Vetterling W T, *et al*. Numerical recipes [M]. Cambridge: Cambridge University Press, 1992.

[41] Parker J S, Doherty B J S, Taylor K T, *et al*. High-energy cutoff in the spectrum of strong-field nonsequential double ionization[J]. Physical Review Letters, 2006, 96(13): 133001.

[42] Armstrong J, Parker S, Taylor T. Double-electron above-threshold ionization resonances as interference phenomena[J]. New Journal of Physics, 2011, 13(1): 013024.

[43] Henrichs K, Waitz M, Trinter F, *et al*. Observation of electron energy discretization in strong field double ionization[J]. Physical Review Letters, 2013, 111(11): 113003.

[44] Gong X C, Song Q Y, Ji Q Y, *et al*. Channel-resolved above-threshold double ionization of acetylene[J]. Physical Review Letters, 2015, 114(16): 163001.